Available online at www.sciencedirect.com
ScienceDirect
The Veterinary Journal 174 (2007) 351–361
The Veterinary Journal
www.elsevier.com/locate/tvjl

Ultrasonographic, computed tomographic and magnetic resonance imaging anatomy of the normal canine stifle joint

Marta Soler [a,*], José Murciano [a], Rafael Latorre [b], Eliseo Belda [a], Maria J. Rodríguez [a], Amalia Agut [a]

[a] Department of Medicine and Surgery, Veterinary School, University of Murcia, 30100 Espinardo, Murcia, Spain
[b] Department of Anatomy, Veterinary School, University of Murcia, 30100 Espinardo, Murcia, Spain

Accepted 10 August 2006

Abstract

Ultrasonographic (US), magnetic resonance (MR) and computed tomographic (CT) images of normal canine stifle joints were obtained and compared with plastinated cross-sectional slices of cadaver specimens from the same dogs. The bony and articular structures were identified and correlated with the three diagnostic imaging modalities. These results provide an atlas of normal cross-sectional US, MR and CT anatomy of the canine stifle, which can be used for the interpretation of stifle images from any of these imaging modalities.

Keywords: Dog; Stifle; Ultrasonography; Magnetic resonance imaging; Computed tomography; Cross-sectional imaging

1. Introduction

In dogs, the stifle is a frequently injured joint. Ligamentous and meniscal damage are frequent injuries and are associated with secondary degenerative changes (Vasseur, 1993). Diagnosis of stifle joint disorders is generally based on a history of lameness, physical examination and radiography (Reed et al., 1995; Kirby, 1993). Diagnostic imaging techniques such as ultrasonography (US), computed tomography (CT) and magnetic resonance imaging (MRI) may be used to further evaluate the bony and soft-tissue structures. The ability of US to image intra-articular soft-tissue structures provides additional information that can be used in conjunction with radiography (Kramer and Gerwing, 1996). Furthermore, US may prove to be useful in the diagnosis of cartilage abnormalities, meniscal tears, muscle, tendon and ligament abnormalities, arthropathies and neoplasia (Reed et al., 1995).

CT and MRI of the stifle allow more sensitive and specific evaluation than radiography alone (Widmer et al., 1994). Both techniques are valuable diagnostic tools in humans, but few veterinary centres have access to these modalities (Baird et al., 1998) due to their high cost. MRI has become the preferred imaging modality for the evaluation of the articular cartilage, menisci and ligaments of synovial joints (Widmer et al., 1994). However, CT is a useful technique for evaluating osseous structures. The ligamentous structures are well observed on three-dimensional CT images, which is utilized in human medicine to guide surgical replacement of the cruciate ligament (Pretorius and Fishman, 1999).

Knowledge of the normal anatomy of the canine stifle joint is essential for the understanding of injuries. To make full use of and interpret the information given by these modern imaging technologies the cross-sectional anatomy has to be studied (Entius et al., 1997). Although normal canine cross-sectional anatomy of the stifle with correlative magnetic resonance (MR) images is available (Baird et al., 1998), to the authors' knowledge, US, CT and MR images

* Corresponding author. Tel.: +34 968 367542; fax: +34 968 364737.
E-mail address: mtasoler@um.es (M. Soler).

1090-0233/$ - see front matter © 2006 Elsevier Ltd. All rights reserved.
doi:10.1016/j.tvjl.2006.08.019

of the canine stifle joint have not been previously reported together.

The aims of the present study were (a) to describe the normal US, CT and MRI anatomy of the canine stifle joint and (b) correlate anatomical cross-sectional slices with the obtained images to facilitate the interpretation of all these images.

2. Materials and methods

Thirty stifle joints were examined using US. After the US study, four of them also underwent MRI and CT examination. Once the CT study was concluded an intra-articular injection of latex was performed and the stifle joints were frozen, sectioned and plastinated.

2.1. Sonographic study

Ultrasonographic scans were carried out on 30 stifle joints of seven adult (4–7 years old) live dogs (14 joints), and from eight cadavers (16 joints), six adults and two immature animals. The US scans of the latter 16 joints were performed immediately after euthanasia. The animals were humanely euthanased for reasons unrelated to stifle joint pathology.

Prior to starting the study, each stifle was clinically assessed by inspection, palpation and dynamic examination (flexion, extension and rotation), and later two orthogonal radiographic views were taken. Only animals without clinical and/or radiological signs of stifle joint disease were included and none of the 15 animals had any evidence of stifle disease on physical and radiographic examination of the stifle joints prior to the study.

As there are no differences between the US appearance of living and dead animals (Reed et al., 1995), all 30 legs were divided into two groups according to the dogs' body weight: Medium (weighing between 10 and 20 kg) and Large (weighing between 20 and 40 kg). These groups were chosen because there are differences in the method of US examination to visualize the structures of the joint depending on the size of the stifle. To standardize the examination the joint was divided into four regions as described by Kramer et al. (1999): suprapatellar, infrapatellar, lateral and medial.

To perform the US examination, the dogs were sedated by IV administration of medetomidine (Domitor, Pfizer) and buprenorphine (Buprex, Schering Plough SA) (5 and 10 μg/kg, respectively). All 30 stifle joints were scanned using a real-time B-mode electronic scanner (Philips P800 Ultrasound System) with a 7.5 MHz linear transducer. To examine the suprapatellar region the acoustic window was located over the tendon of the quadriceps femoris muscle. To produce an infrapatellar longitudinal view, the transducer was placed cranially on the straight patellar ligament. The cruciate ligaments were examined on mid sagittal images with the leg in full flexion. For better visibility of the cranial cruciate ligament it was necessary to rotate the transducer 10–20° laterally in a sagittal section. To evaluate the lateral and medial regions of the joints, the transducer was placed either laterally and medially to the patellar ligament with the joint flexed to produce sagittal sections (Kramer et al., 1999). The sonographic anatomy and the normal echogenicity of the different structures were determined.

2.2. MRI study

After the US scans of the specimens had been performed, MRI was carried out in four selected joints (two adults and two immatures), within 2 h of euthanasia to minimize the possibility of post mortem changes interfering with the images. Dogs were positioned in dorsal recumbency with the hindlimbs extended. MRI images of the stifle joints were obtained in sagittal, dorsal and transverse planes using a 0.5 Tesla (General Electric Medical System) magnet and a solenoidal human extremity coil. The sagittal plane was performed slightly rotated, orientated parallel to the medial surface of the lateral femoral condyle.

A T1-weighted spin echo (SE) sequence (TR = 420 ms; TE = 25 ms) was used to obtain the best anatomical detail of the soft-tissues of the joint and a T2*-weighted gradient echo (GE) sequence (TR = 540 ms; TE = 22 ms) was selected to maximize signal and contrast between articular cartilage and the adjacent tissues. The signal intensity of each structure was studied.

2.3. CT study

CT of the four stifle joints was performed immediately following MRI scanning, using a helical CT scanner (CT HiSpeed CT/e Dual; General Electric Medical System). Technical factors were 25–30 mAs and 120 kVp. Contiguous 1 mm transverse slices were made from a level proximal to the femoral condyles to the proximal tibia. To enhance bony structures a wide window was used (window width: 200 Hounsfield units; window level: 1700 Hounsfield units) and for soft-tissue structures a narrow window was chosen (window width: 30 Hounsfield units; window level: 300 Hounsfield units). Each CT image set was volume rendered to provide a three-dimensional (3D) representation of the stifle.

The original CT data were transferred as DICOM images to an image analysis workstation (GE Advantage Workstation 3.1) to perform the image analysis. The original transverse slices were reformatted into the sagittal and dorsal planes. The window was also adjusted as required to better define bone margins. The opacity of all structures was observed and noted.

2.4. Anatomical study

At the conclusion of the CT examination of the four pelvic limbs, the stifle joints were injected with coloured latex. After the injection the limbs were frozen at −30 °C for 48 h.

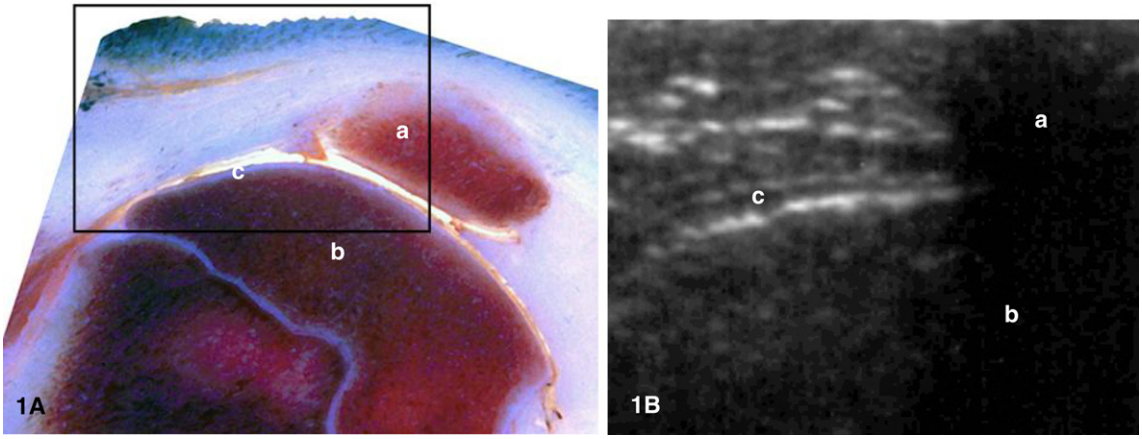

Fig. 1. Cross-sectional anatomical image (A) and US image (B) at the level of the femoral trochlea. (a) Patella, (b) femur and (c) articular cartilage.

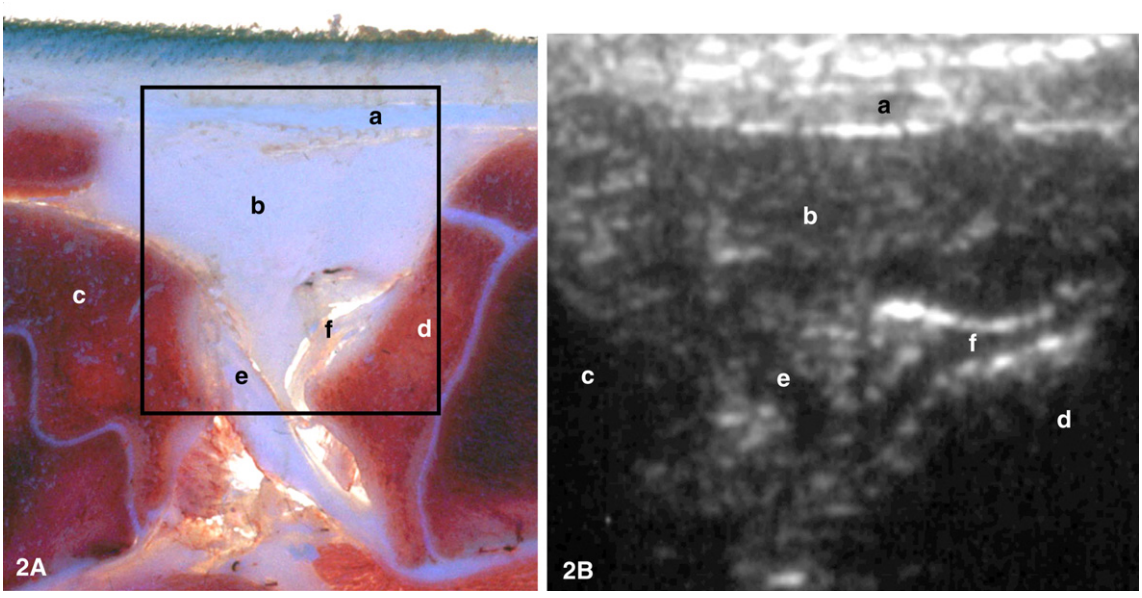

Fig. 2. Cross-sectional anatomical image (A) and US image (B) at the level of the intercondylar notch. (a) Patellar ligament, (b) infrapatellar fat pad, (c) femur, (d) tibia, (e) caudal cruciate ligament and (f) cranial cruciate ligament.

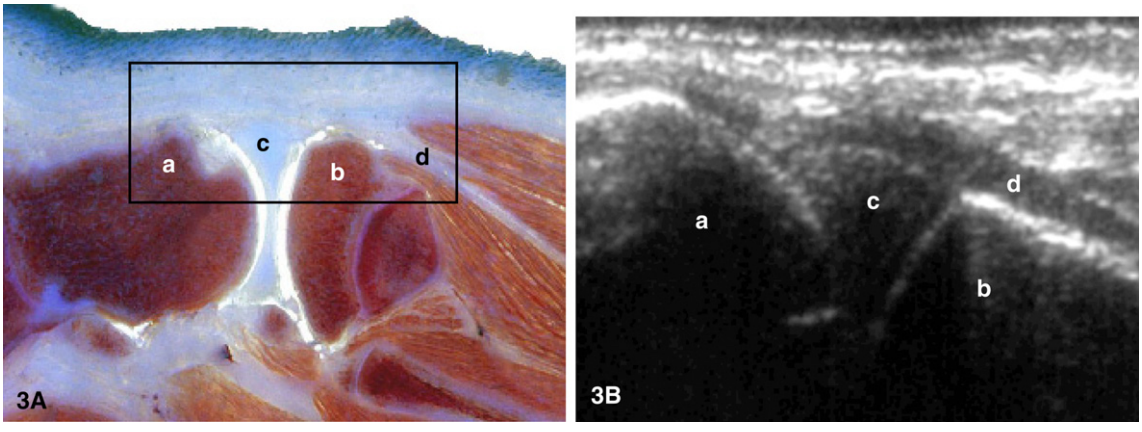

Fig. 3. Cross-sectional anatomical image (A) and US image (B) at the level of the lateral ridge of the femoral trochlea. (a) Lateral femoral condyle, (b) lateral tibial condyle, (c) cranial horn of the lateral meniscus and (d) tendon of the long digital extensor muscle.

Then, the frozen pelvic limbs were sectioned in a block including only the stifle joint and returned to the freezer, this time at −70 °C. Forty-eight hours later, sagittal, dorsal and transverse cryosections were made with a high-speed band saw at the desired thickness of 2–4 mm. The sections were plastinated using P-40 and E-12 techniques (Latorre et al., 2002; Von Hagens et al., 1987). Photographs of each slice were taken. The plastinated slices were used to facilitate an accurate interpretation of the anatomical structures and were compared to the corresponding US, MR and

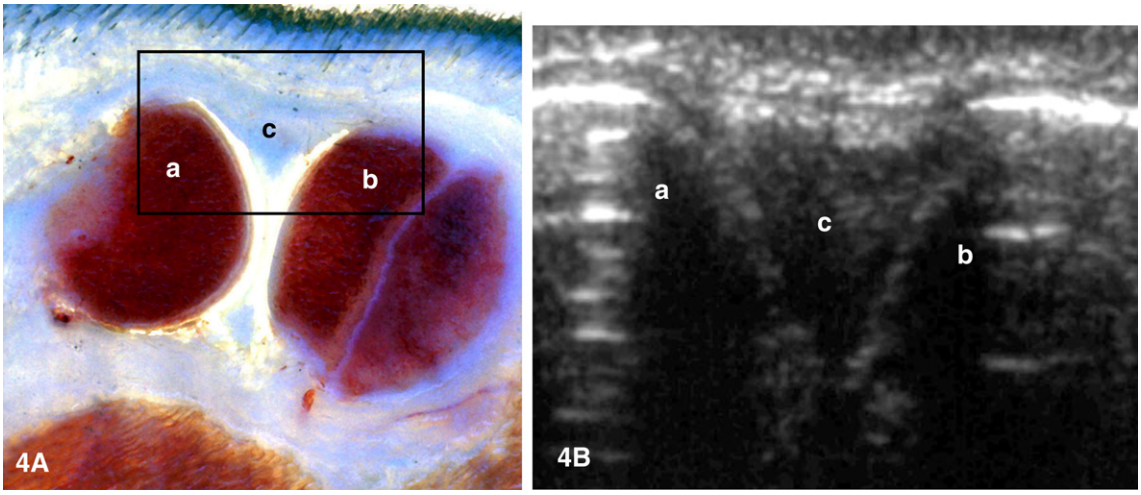

Fig. 4. Cross-sectional anatomical image (A) and US image (B) at the level of the medial ridge of the femoral trochlea. (a) Medial femoral condyle, (b) medial tibial condyle and (c) cranial horn of the medial meniscus.

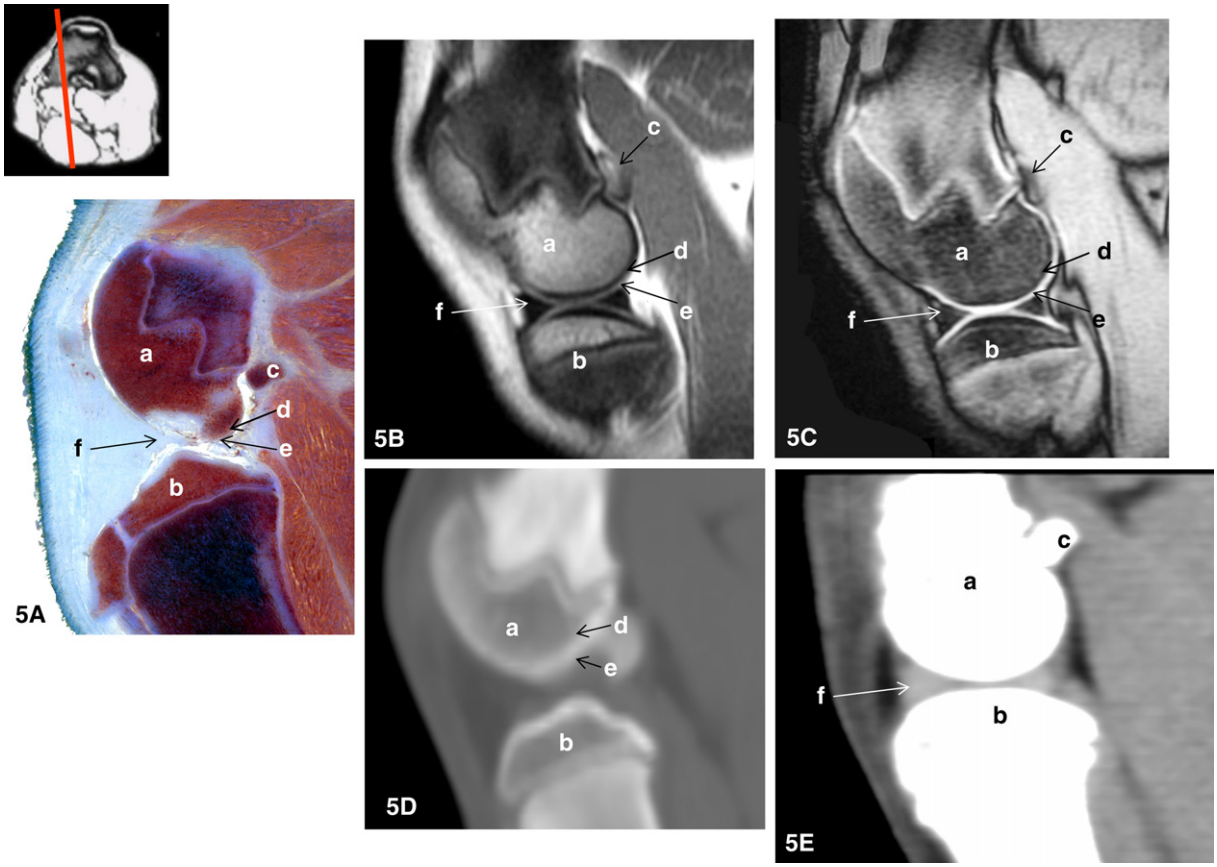

Fig. 5. Cross-sectional anatomical image (A); sagittal T1 weighted MRI image (B); T2*-gradient-echo MR image (C); Bone window CT image (D) and soft-tissue window CT image (E) at the level of the medial femoral condyle. (a) Medial femoral condyle, (b) medial tibial condyle, (c) medial sesamoid bone of the gastrocnemius muscle, (d) subchondral bone of the femur, (e) articular cartilage of the femur and (f) cranial horn of the medial meniscus.

CT images for identification and confirmation of each anatomical structure.

3. Results

3.1. Sonographic study

For better interpretation of the different structures of the stifle joint, figures corresponding to the cross-section of each region are presented. In the suprapatellar region, the patella appeared as a hyper-reflective, convex, smooth structure with acoustic shadowing. The articular cartilage of the femoral condyles was seen as a smooth, distinct, hypoechoic line between the echogenic cartilage–femoral bone interface and the echogenic cartilage–soft-tissue interface (Fig. 1). The tendon of the quadriceps femoris muscle was hypoechoic with fibrillar structure and a hyper-reflective peritendon. These structures were seen in all joints (30/30). In the infrapatellar region, the patellar ligament was identified in all cases (30/30) as a homogeneous hyper-reflective fibrillar structure, which appeared hyperechoic to the patellar fat pad, with a peritendon that was seen as a hyper-reflective solid line (Fig. 2).

In all joints, the cranial cruciate ligament was seen as a hypoechoic band when compared to the patellar ligament. It extended from the cranial margin of the tibial plateau to the region between the femoral condyles. In all 12 joints from large dogs, the caudal cruciate ligament was identified with maximal knee extension rotating the probe about 15° medially from the initial position. The caudal cruciate ligament was visualized at the point of its femoral attachment, toward the popliteal notch of the tibia. It appeared as a hypoechoic band, but isoechoic to the cranial cruciate ligament. In all of the joints from the group of medium sized dogs (18/30), both caudal and cranial cruciate ligaments were seen at the same time, with the joint in full flexion. The cruciate ligaments appeared forming a V-like shape, clearly evident in 11/18 joints, whereas in the other five joints the caudal cruciate ligament was not as clear due to the narrow space between the femoral condyles limiting transducer access and visibility of the structure (Fig. 2).

The lateral and medial regions were demarcated proximally by the lateral and medial femoral condyles and distally by the lateral and medial tibial condyles. With evaluation of the lateral and medial regions, the menisci were identified in all the joints as homogeneous triangular structures with moderate echogenicity which were hypoechoic when compared with the patellar ligament (Figs. 3 and 4). The difference observed between sides was the presence of the long digital extensor tendon immediately super-

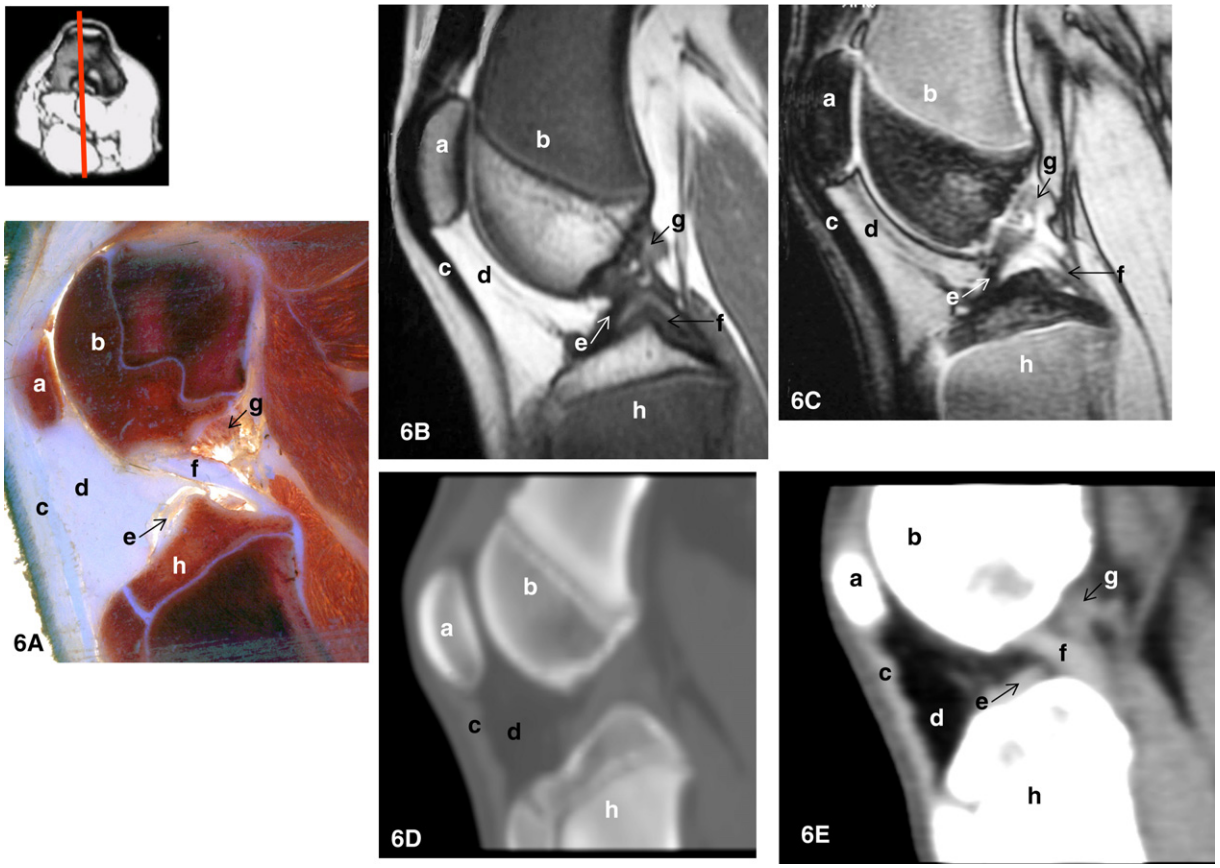

Fig. 6. Cross-sectional anatomical image (A); sagittal T1 weighted MRI image (B); T2* GE MRI image (C); Bone window CT image (D) and soft-tissue window CT image (E) at the level of the intercondylar notch. (a) Patella, (b) femur, (c) patellar ligament, (d) infrapatellar fat pad, (e) cranial cruciate ligament, (f) caudal cruciate ligament, (g) meniscofemoral ligament and (h) tibia.

ficial to the lateral meniscus. It was a hypoechoic solid line surrounded by a hyper-reflective outpouching of the synovial membrane of the joint capsule (Fig. 3). It was identified in all the cases, seen reasonably well in 12 animals of the medium group and very well seen in the other 18 cases of medium and large groups (18/30).

Collateral ligaments, meniscal and intermeniscal ligaments were not identified. All the structures identified ultrasonographically were correlated in the anatomical sections.

3.2. Magnetic resonance imaging

Six cadaver cross-sections with their corresponding MRI and CT images were selected. The sagittal images began at the medial aspect of the stifle joint and continued laterally through the joint (Figs. 5 and 6). The transverse images began at the level of the proximal femoral trochlea and continued distally (Figs. 7 and 8) and the dorsal images began at the level of the femoral intercondylar notch and continued caudally (Figs. 9 and 10).

Joint structures studied in MR images were correlated with structures identified in the corresponding anatomical sections. The patella had moderate signal intensity due to the trabecular bone on SE T1-weighted images. On GE T2*-weighted images it had a lower signal intensity being almost isointense to the patellar ligament. In the three planes and in both sequences the surface of the patella was surrounded by a low intensity signal corresponding to the cortical bone (Figs. 6 and 7).

Ligaments, tendons and menisci were seen with low homogeneous signal intensity in both sequences. The articular cartilage had a similar low signal intensity in T1-weighted SE sequence, but not in T2*-weighted gradient echo images where the cartilage was presented with high intensity signal (Widmer et al., 1994). In both sequences the signal of the articular cartilage was separated from trabecular bone by a hypointense line that represented subchondral bone (Figs. 5 and 7). The menisci were easily identified as triangular shaped structures, with the sharp part medially and the thick border laterally, in the dorsal and sagittal planes, however, they were not clearly seen

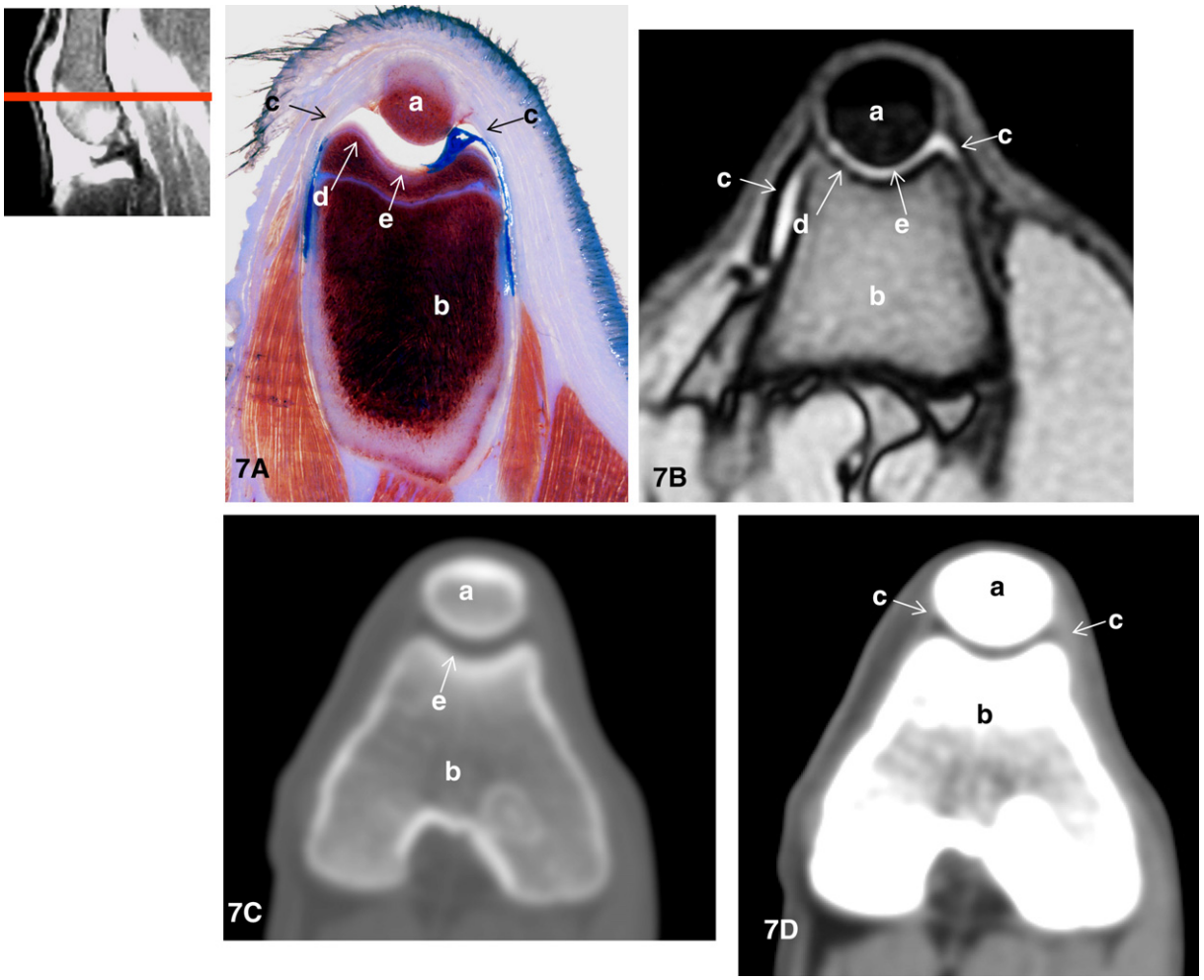

Fig. 7. Cross-sectional anatomical image (A); transverse T2*-gradient-echo MR image (B); Bone window CT image (C) and soft-tissue window CT image (D) at the level of the proximal femoral trochlea. (a) Patella, (b) femur, (c) articular capsule, (d) subchondral bone of the femur and (e) articular cartilage of the femur.

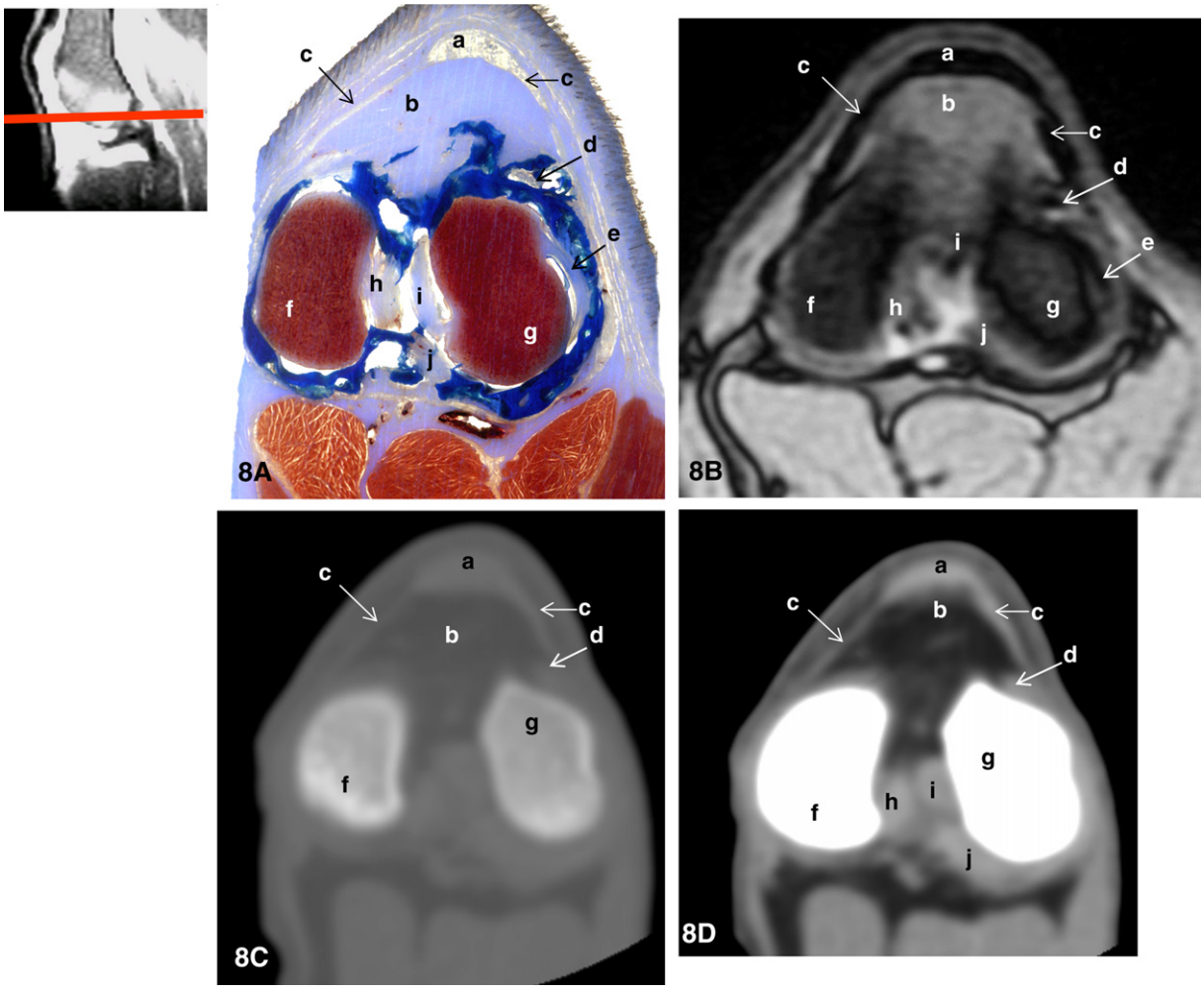

Fig. 8. Cross-sectional anatomical image (A); transverse T2*-gradient-echo MRI image (B); Bone window CT image (C) and soft-tissue window CT image (D) at the level of the intercondylar femoral fossa. (a) Patellar ligament, (b) infrapatellar fat pad, (c) articular capsule, (d) tendon of the long digital extensor muscle, (e) tendon of the popliteal muscle, (f) medial femoral condyle, (g) lateral femoral condyle, (h) caudal cruciate ligament, (i) cranial cruciate ligament and (j) meniscofemoral ligament.

in the transverse plane due to the slice thickness and to its own shape (Figs. 5, 9 and 10). The cranial and caudal cruciate ligaments were identified in all three planes. They were seen as two low intensity bands, although they could not be seen in its entirety due to their oblique orientation within the joint (Figs. 6 and 8–10). The meniscofemoral ligament and the medial and lateral collateral ligaments were readily seen on the dorsal plane as linear low signal intensity bands (Figs. 9 and 10). The tendon of the long digital extensor muscle could be identified on the sagittal and transverse planes (Fig. 8). The tendon of the popliteal muscle was seen on all three planes, however, the best images were on transverse plane (Fig. 8). Both tendons had low signal intensity.

3.3. Computed tomography

Joint structures studied in CT images were matched and correlated with structures identified in the corresponding anatomical sections. When a soft-tissue window was used, bones appeared hyperdense while tendons, ligaments and muscles were represented by variable density. Synovial fluid and blood vessels were hypodense. Muscle tissues had the lowest density and tendons and ligaments were denser than the muscles.

The patellar ligament, cruciate ligaments, meniscofemoral ligament, and menisci all had a similar density, hyperdense to the patellar fat pad, and could be seen on the same planes as described in MR images. The collateral ligaments, the tendon of the long digital extensor muscle and the tendon of the popliteal muscle were not clearly identified.

Images made with a bone window produced good delineation between cortex and medulla. The trabecular pattern and the physis were well depicted and the articular cartilage was seen as a hyperdense line (Figs. 5 and 7). With volume-rendering reconstruction techniques, 3D-CT images were produced, rotated and sectioned as desired. Overlaying anatomical parts could be substracted thereby allowing evaluation of the patellar and cruciate ligaments, the ten-

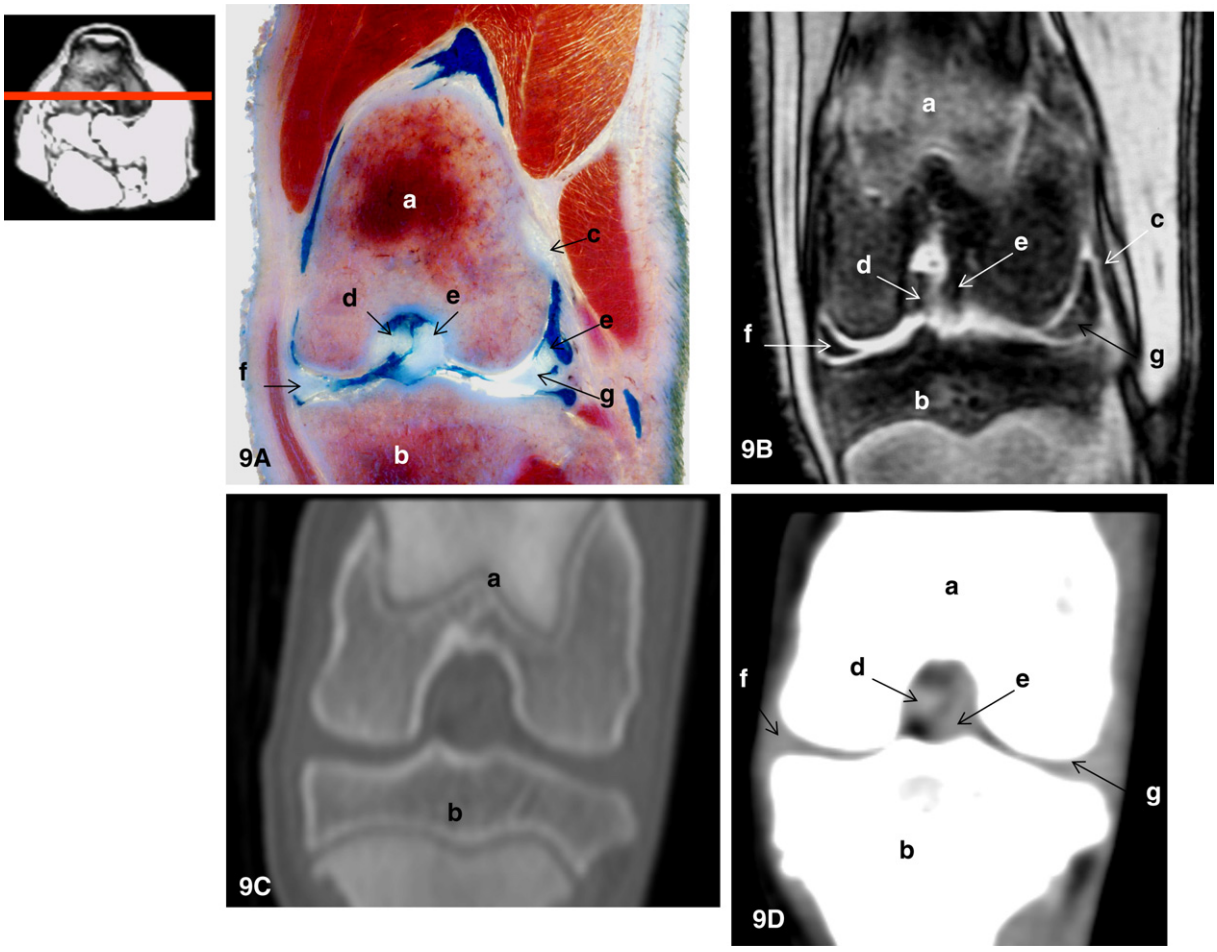

Fig. 9. Cross-sectional anatomical image (A); dorsal T2* GE MR image (B); Bone window CT image (C) and soft-tissue window CT image (D) at the level of the intercondylar notch. (a) Femur, (b) tibia, (c) lateral collateral ligament, (d) caudal cruciate ligament, (e) cranial cruciate ligament, (f) medial meniscus, (g) lateral meniscus.

don of the long digital extensor muscle, menisci and bony surfaces (Figs. 11 and 12).

4. Discussion

Trauma to the stifle joint may cause rupture of the ligamentous structures. The highest incidence of damage is to the cranial cruciate ligament and menisci (Asseheuer and Sagger, 1997). Diagnosis of stifle joint disorders is generally based on a history of lameness, physical examination, radiography, arthrography, US and MRI.

Disease affecting the stifle joint is suspected when the animal shows lameness, pain and/or swelling of the joint. Diagnostic imaging techniques are used to investigate the source of the pathology and radiography is the most common method used. If there are no radiographic signs of stifle joint disease and the animals do not show clinical signs, an underlying pathology is unlikely. The animals included in this study were considered normal for the purpose of our research as they were chosen based on the lack of clinical and radiographic findings.

CT and MRI are used less widely in veterinary medicine than US. The main reasons are cost and the need for general anaesthesia. Ultrasound is a safe, non-invasive, low cost procedure which is well tolerated by the animal and therefore can be performed in the conscious patient or under light sedation (Kramer et al., 1999). It can be useful and clinically applicable for the evaluation of most intra-articular structures (Kramer et al., 1999; Reed et al., 1995). There are however several major limitations associated with US imaging that limit its usefulness for the evaluation of the stifle joint. Individual US images represent only a portion of the complete cross-sectional anatomy for any given level of the body. Furthermore, the US beam is unable to sufficiently penetrate structures that contain mineral, and in very small animals, the joint space is too narrow and it can be difficult to reproduce these findings due to the size of the joints and the size of the scanner (Kramer et al., 1999). In this study, we used a greater number of joints for US than for CT and MRI due to those limitations to perform the ultrasonographic examinations in the stifle of small breed dogs, so we could standardize the

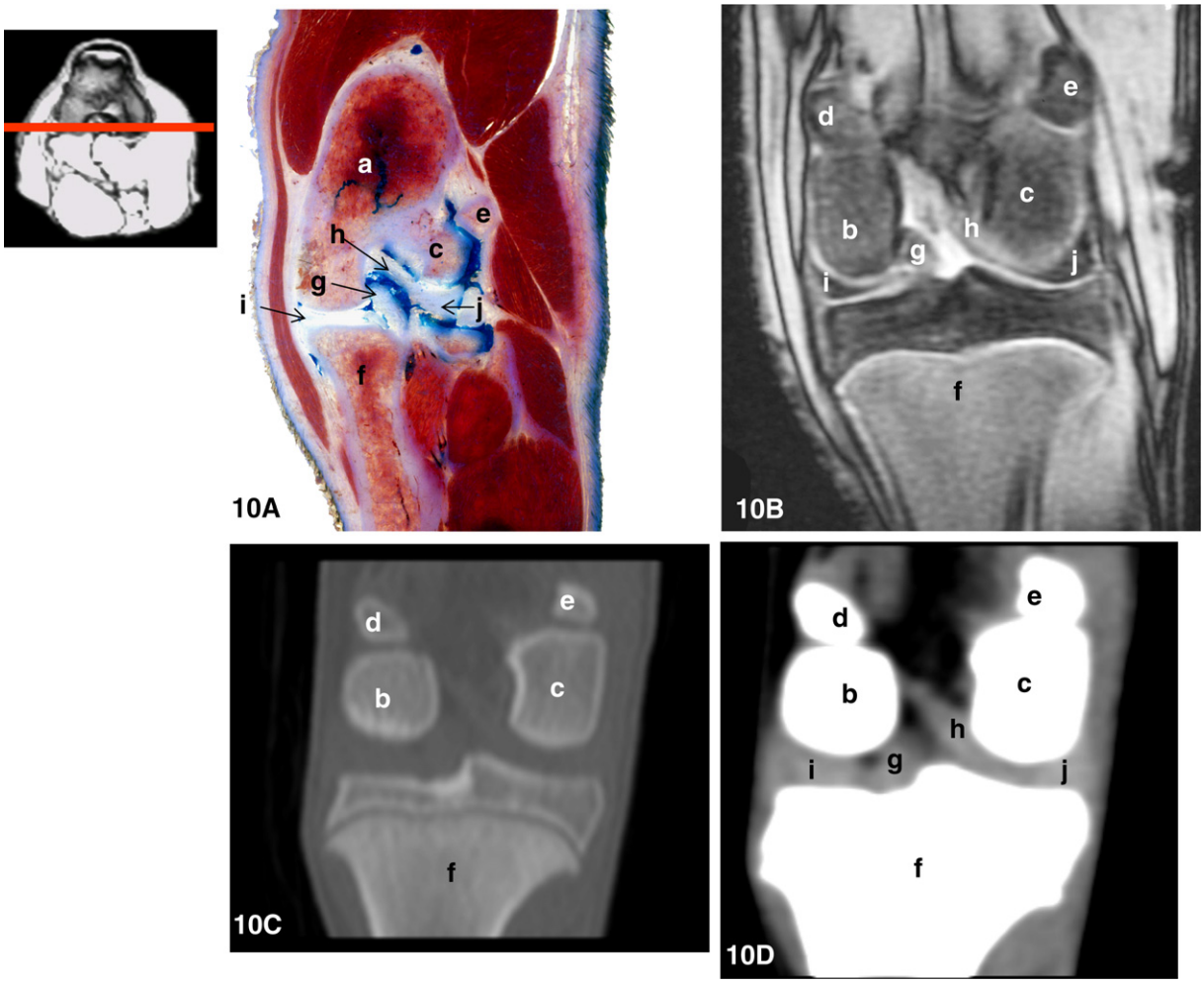

Fig. 10. Cross-sectional anatomical image (A); dorsal T2* GE MRI image (B); Bone window CT image (C) and soft-tissue window CT image (D) at the level of the femoral condyles. (a) Femur, (b) medial femoral condyle, (c) lateral femoral condyle, (d) medial sesamoid bone of the gastrocnemius muscle, (e) lateral sesamoid bone of the gastrocnemius muscle, (f) tibia, (g) caudal cruciate ligament, (h) meniscofemoral ligament and (j) lateral meniscus.

results of the images obtained. Finally, compared with CT and MRI, US images have relatively poor resolution and soft tissue contrast (Samii et al., 1998).

All major soft-tissue structures are clearly outlined both on CT and MR images. Our results are in agreement with the conclusions of Kaser-Hotz et al. (1994); in their paper on CT and MRI of the equine carpus, the authors stated that the techniques allow more specific diagnosis of ligamentous, tendinous and synovial abnormalities in the joint than is possible with US or radiography.

In our study, we have found that all of the anatomical structures identified in the cross-sections were correlated in the US, MRI and CT images with the exception of the collateral ligaments that could not be seen by US, and the tendon of the long digital extensor muscle, the tendon of the popliteal muscle and the collateral ligaments that were not clearly identified in the CT images.

CT and MRI provided excellent images of stifle joint anatomy. The most obvious difference comparing CT with MR images, was the greater soft-tissue contrast demonstrated in MR images. Tendons and ligaments were more clearly defined in the MR images, but tissue texture was more readily appreciated using CT (Kaser-Hotz et al., 1994). The articular cartilage was visualized on CT images where the bone window was used as a hyperdense line, although it was best delineated on MR images, especially on T2*-weighted gradient echo images where it presented a high intensity signal.

The better soft-tissue contrast seen on MR images may not be sufficient enough reason to decide in favour of using CT or MRI, because CT scans also provide diagnostic soft-tissue and bone images (Kaser-Hotz et al., 1994). Although MRI is the preferred modality for evaluating the ligaments and menisci of the stifle, helical CT with multiplanar reconstruction and volume rendering has been used to guide surgical replacement of cruciate ligaments (Pretorius and Fishman, 1999). Helical CT has the potential to reduce the time of the examination considerably (Samii and Dyce, 2004), and the procedure may be performed in animals that are deeply sedated (De Rycke et al., 2003).

CT images can be manipulated on the viewing console to demonstrate bone or soft-tissue detail. Images can also

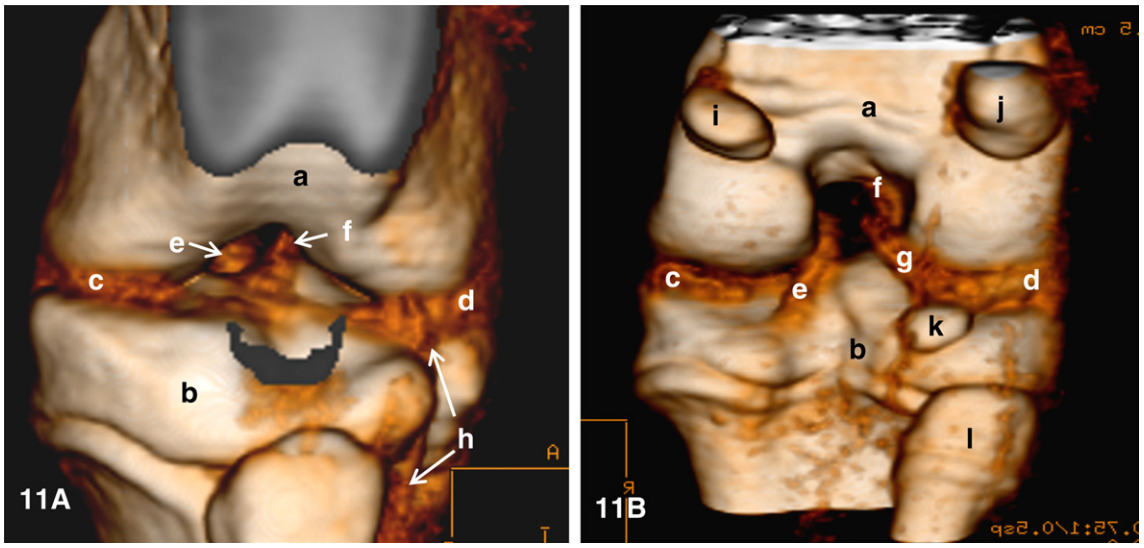

Fig. 11. Volume-rendered images of the dorsal (A) and caudal (B) views of the stifle joint. (a) Femur, (b) tibia, (c) medial meniscus, (d) lateral meniscus, (e) caudal cruciate ligament, (f) cranial cruciate ligament, (g) meniscofemoral ligament, (h) long digital extensor tendon, (i) medial sesamoid bone of the gastrocnemius muscle, (j) lateral sesamoid bone of the gastrocnemius muscle, (k) sesamoid bone of the popliteal muscle and (l) fibula.

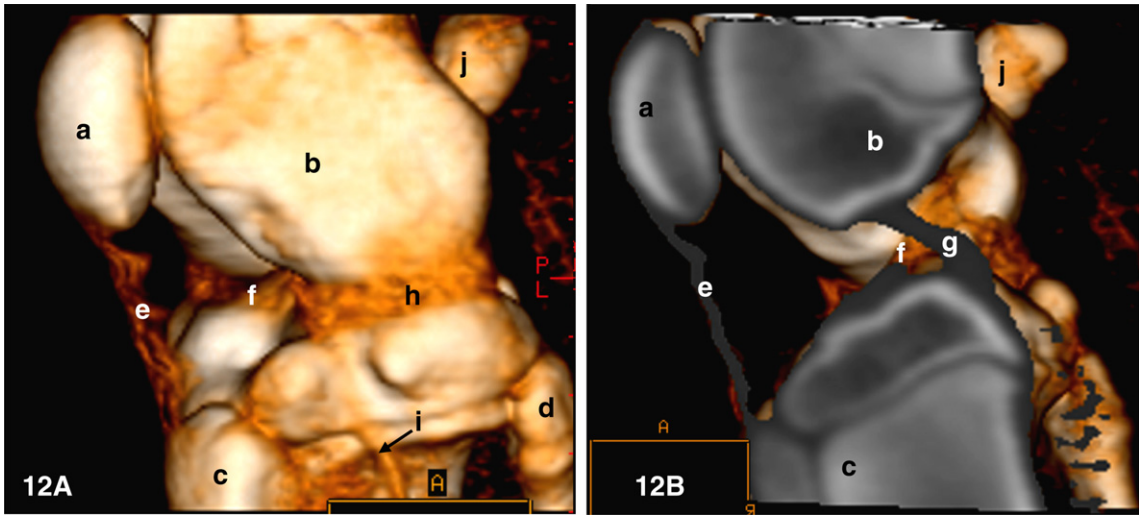

Fig. 12. Volume rendered images of the lateral view of the stifle joint (A) and subtracting overlaying anatomical parts (B). (a) Patella, (b) lateral femoral condyle, (c) tibia, (d) fibula, (e) patellar ligament, (f) cranial cruciate ligament, (g) caudal cruciate ligament, (h) lateral meniscus, (i) long digital extensor tendon and (j) lateral sesamoid bone of the gastrocnemius muscle.

be formatted into different image planes (Berquist, 1997). The multidetector CT technology with its ability to increase the speed of CT examinations and its flexibility in acquisition and reconstruction of images, offer further clinical applications in veterinary medicine (Bertolini et al., 2003).

The lack of familiarity with the normal cross-sectional anatomy is a major factor slowing the learning process for interpreting US, CT and MR images; the easiest way to learn cross-sectional anatomy is directly from cross-sectional images (Samii et al., 1998). Therefore, the plastinated slices used in this study facilitated an accurate interpretation of the anatomical structures on corresponding US, MR and CT images.

Based on our results, all of the joint structures of the canine stifle can be better identified and evaluated by MRI. Most of the soft-tissue structures that were seen on MRI were also identified on CT images when a soft-tissue window was used, but never with the definition that MR images offer. Ultrasonographic images are helpful to evaluate ligaments, tendons and menisci, although the animal's size can lead to limitations in visualizing these structures.

In conclusion, this study gives anatomical information on the canine stifle joint, which can be useful in both clinical and research use. This information can serve as a baseline reference for evaluation of US, CT and MRI scans of the canine stifle joint and may be used to assist clinicians in the interpretation of pathological conditions of this joint.

Acknowledgements

The authors wish to thank Dr. Heike Rudorf and Dr. Robert W. Henry for their critical revision of the manuscript.

References

Asseheuer, J., Sagger, M., 1997. Stifle joint. In: Assheuer, J., Sagger, M. (Eds.), MRI and CT Atlas of the Dog. Blackwell Science, Berlin, Germany, pp. 266–269.

Baird, D.K., Hathlock, J.T., Rumph, P.F., Kincaid, S.A., Visco, D.M., 1998. Low-field magnetic resonance imaging on the canine stifle joint: normal anatomy. Veterinary Radiology and Ultrasound 39, 87–97.

Berquist, T.H., 1997. Imaging of articular pathology: MRI, CT, Arthrography. Clinical Anatomy 10, 1–13.

Bertolini, G., Furlanello, T., Caldin, M., 2003. Preliminary experiences and clinical applications of multislice-CT in small animal practice. In: Proceedings of the Autumn Meeting, European Association of Veterinary Diagnostic Imaging, Cambridge, UK, p. 29.

De Rycke, L.M., Saunders, J.H., Gielen, I.M., Van Bree, H.J., Simoens, P.J., 2003. Magnetic resonance imaging, computed tomography, and cross-sectional views of the anatomy of normal nasal cavities and paranasal sinuses in mesaticephalic dogs. American Journal of Veterinary Research 9, 1093–1098.

Entius, C.A.C., van Rijn, R.R., Holstege, J.C., Stoeckart, R., Zwamborn, A.W., 1997. Correlating sheet plastinated slices, computed tomography images and magnetic resonance images of the pelvic girdle: a teaching tool. Acta Anatomica 158, 44–47.

Kaser-Hotz, B., Sartoretti-Schefer, S., Weiss, R., 1994. Computed tomography and magnetic resonance imaging of the normal equine carpus. Veterinary Radiology and Ultrasound 6, 457–461.

Kirby, B.M., 1993. Decision-making in cranial cruciate ligament ruptures. The Veterinary Clinic of North America (Small Animal Practice) 23, 797–819.

Kramer, M., Gerwing, M., 1996. Die bedeutung der sonographie in der orthopadie beim hund. Berliner und Münchener Tierärztliche Wochenschrift 109, 130–135.

Kramer, M., Stengel, H., Gerwing, M., Schimke, E., Sheppard, C., 1999. Sonography of the canine stifle. Veterinary Radiology and Ultrasound 40, 282–293.

Latorre, R.M., Reed, R.B., Gil, F., López-Albors, O., Ayala, M.D., Martínez-Gomariz, F., Henry, R.W., 2002. Epoxy impregnation without hardener: to decrease yellowing, to delay casting, and to aid bubble removal. Journal of the International Society for Plastination 17, 17–22.

Pretorius, E.S., Fishman, E.K., 1999. Volume-rendered three-dimensional spiral CT: musculoskeletal applications. Radiographics 19, 1143–1160.

Reed, A.L., Payne, J.T., Constantinescu, G.M., 1995. Ultrasonographic anatomy of the normal canine stifle. Veterinary Radiology and Ultrasound 36, 315–321.

Samii, V.F., Dyce, J., 2004. Computed tomographic arthrography of the normal canine stifle. Veterinary Radiology and Ultrasound 45, 402–406.

Samii, V.F., Biller, D.S., Koblik, P.D., 1998. Normal cross-sectional anatomy of the feline thorax and abdomen: comparison of computed tomography and cadaver anatomy. Veterinary Radiology and Ultrasound 39, 504–511.

Vasseur, P.B., 1993. Stifle joint. In: Slatter, D. (Ed.), Textbook of Small Animal Surgery, second ed. WB Saunders, Philadelphia, United States, pp. 1817–1865.

Von Hagens, G., Tiedemann, K., Kriz, W., 1987. The current potential of plastination. Anatomy and Embryology 175, 411–421.

Widmer, W.R., Buckwalter, K.A., Braunstein, E.M., Hill, M.A., O'Connor, B.L., Visco, D.M., 1994. Radiographic and magnetic resonance imaging of the stifle joint in experimental osteoarthritis of dogs. Veterinary Radiology and Ultrasound 35, 371–383.